INSTITUTE FOR NUCLEAR STUDY
UNIVERSITY OF TOKYO
Tanashi, Tokyo 188
Japan

INS-Rep.-605
Sept. 1986

INS GAS-FILLED RECOIL ISOTOPE SEPARATOR

M. MIYATAKE*, T. NOMURA, H. KAWAKAMI, J. TANAKA, M. OYAIZU,
K. MORITA, T. SHINOZUKA, H. KUDO, K. SUEKI and Y. IWATA

INS-Rep.-605
Sept. 1986

INS GAS-FILLED RECOIL ISOTOPE SEPARATOR

M. MIYATAKE*, T. NOMURA, H. KAWAKAMI, J. TANAKA and M. OYAIZU

Institute for Nuclear Study, University of Tokyo, Tanashi, Tokyo, 188 Japan

K. MORITA

Cyclotron Laboratory, The Institute of Physical and Chemical Research, Wako, Saitama, 351 Japan

T. SHINOZUKA

Cyclotron Radioisotope Center, Tohoku University, Sendai, Miyagi, 982 Japan

H. KUDO

Department of Chemistry, Niigata University, Igarashi, Niigata, 950-21 Japan

K. SUEKI

Department of Chemistry, Tokyo Metropolitan University, Setagaya, Tokyo, 158 Japan

and

Y. IWATA

Department of Physics, Hiroshima University, Nakaku, Hiroshima, 730 Japan

*present address; Laboratory of Nuclear Studies, Faculty of Science, Osaka University, Toyonaka, Osaka, 560 Japan

Abstract

The characteristics and performance of a small sized gas-filled recoil isotope separator recently made at INS are described. The total efficiency and the $\Delta B\rho/B\rho$ values have been measured using low velocity ^{16}O, ^{40}Ar and ^{68}As ions and found to be 10 and 5 %, respectively. The Z-dependence of the mean charge is discussed.

1. Introduction

A gas-filled recoil isotope separator (GARIS) has been made by the SF cyclotron in the Institute for Nuclear Study, University of Tokyo. The present GARIS mainly aims at efficient collection of reaction products by separating them from beam particles for the study of short-lived nuclei.

This separation method was developed by Cohen and Fulmer [1] in 1958 and later in Jülich [2] mainly for the study of fission products. Bacho et al. [3] at Dubna and recently Ghiorso et al. [4] at LBL applied this method to the study of nuclei produced in heavy ion reactions. These separators have characteristics of high total efficiency (~20%) and short separation time (~1μs).

The principle of GARIS is as follows. Reaction products recoiled out of a target have broad distributions both in charge and momentum. When they enter a dipole magnetic field with gas of low pressure, they follow an average trajectory corresponding to their momenta and an average charge ($\bar{q}$) defined by their multiple collision with gas atoms. Because the average charge is roughly propotional to momentum, the average trajectory is almost

independent of the initial distributions of momentum and charge states, and depends only on their mass (A) and atomic numbers (Z). That is,

$$q=(v/v_0)Z^{\alpha}, \qquad (1)$$

in which v is the velocity of the recoiled atom and v_0 is the Bohr velocity ($v_0=c/137$). The value of α is 1/3 according to Bohr [5], but is empirically about 0.6 for ions moving with relatively low velocities as will be discussed later. The magnetic rigidity ($B\rho$) can be written by,

$$B\rho = 0.02268A(v/v_0)\bar{q}^{-1} \quad (\mathrm{Ts\cdot m})$$
$$\propto A/Z^{\alpha} \qquad (2)$$

2. Characteristics

The present GARIS consists of Q-Q-D-Q-Q configuration as schematically shown in fig. 1. The chracteristics of dipole and quadrupole magnets are listed in table 1. The dispersion of the GARIS has been estimated to be 7.14 mm for 1% of $\Delta B\rho/B\rho$. The distance between the target and the input boundary of the dipole magnet is 1.6 m, whereas the distance between the output boundary and the focussing point is 1.7 m.

A region filled by helium gas is separated from the vaccuum region by a thin nickel foil of 16 mm in diameter, which is placed just before the target position upstream. The pressure of He is measured by a capacitance manometer at the detector chamber and is controlled remotely with a solenoid-type gas-inlet valve at the target chamber. The vertical and horizontal acceptance angles are usually 70 mr and 50 mr, respectively.

3. Performance

The present GARIS has been tested first by using ^{16}O and ^{40}Ar beams which pass through the Ni-window and have thus significant momentum spread. Later we have also tested it by using the reaction $^{58}Ni(^{12}C, pn)^{68}As$ at 44 Mev, in which the Ni-window is used as a target. The collection efficiency of the system as well as the $B\rho$-resolution, $\Delta B\rho/B\rho$, have been measured versus the gas pressure and are compared with the theoretical estimates.

The various experimental parameters such as beam energies and momentum spreads are listed in table 2. In the case of ^{16}O and ^{40}Ar beams the beam intensity was measured by a Farady cup set at the focal plane. For example, the measured charge-distribution spectra of ^{16}O (E=33 MeV) are shown in fig. 2. In the case of ^{68}As, the 1016 keV γ-ray following the β-decay was measured with a 80 cm^3 Ge detector placed at the detector chamber. The results are shown in figs. 3 - 5. For example, in the case of ^{40}Ar beam, the minimum value of the $B\rho$-resolution is 5 % at the He pressure of 3 torr.

It is known that the $B\rho$-resolution are mainly determined by statistics of charge-changing collision, multiple scattering, velocity dispersion and beam optics. We estimated these effects in the same way as described in ref. [6]. The effect of energy loss of ions in helium gas was also taken into account.

A contribution of charge-changing collision is given by

$$\Delta B\rho/B\rho = 5.51 \times 10^3 (\Delta q/\bar{q})/\sqrt{p\ell\Omega_{eff}}, \qquad (3)$$

in which Δq is a half-width of a charge distribution, p and ℓ being pressure of He in torr and a length of the magnetic field

in cm. Ω_{eff} represents an effective experimental charge-changing cross section.

The multiple scattering contribution can be given by a half width of lateral spread ($\rho_{1/2}$) and the dispersion of GARIS (D) as

$$\Delta B\rho/B\rho = \rho_{1/2}/D, \qquad (4)$$

in which $\rho_{1/2}$ is obtained from ref. [7].

The effects of velocity dispersion and beam optics have been also calculated by a program code. Their contributions to the $\Delta B\rho/B\rho$ values were found to be 3 % and 0.2 %, respectively, in the case of ^{40}Ar.

The calculated curves of $\Delta B\rho/B\rho$ are shown by solid curves in figs. 3 - 5. Note that values of Ω_{eff} for ^{40}Ar, ^{16}O and ^{68}As ions were chosen to be respectively 7.7, 25 and 3.2 % of those calculated by using an unified empirical formula for a single electron capture [8] in order to obtain the best fits. The above values are consistent with those given in ref. [6].

The efficiency of the GARIS is defined as ratio of the amount of radio-activity of interest collected at the focal plane and that recoiled out of the target. The total efficiency was found to be about 10 % for the case of ^{68}As under the condition that the width of vertical slit in front of the Al-foil catcher at the focal plane was 50 mm.

4. Z-dependence of mean charges

The measured average charges ($\bar{q}$) at the helium pressure corresponding to the minimum $B\rho$-resolution are listed in the last

column of table 2. Petrov et al. [9] have shown that $\bar{q}$ of ions moving in helium gas with relatively low velocities ($v/v_0=4$) is proportional to $Z^{0.57}$ for $36 \leq Z \leq 54$. In order to see if this holds for smaller Z values, the present data are plotted in fig. 6 together with the results of ref. [9]. Note that the present values of $\bar{q}$ have been transformed, for comparison, into those expected at $v/v_0=4$ by using eq. (1). It is clear that the $Z^{0.57}$ dependence of $\bar{q}$ holds well down to Z=8.

References

[1] B. L. Cohen and C. B. Fulmer, Nucl. Phys. 6(1958)547.

[2] H. Lawin, J. Eidens, J. W. Borgs, R. Fabbri, J. W. Grüter, G. Joswig, T. A. Khan, W. D. Lauppe, G. Sadler, H. A. Selic, M. Shaanan, K. Sistemich and P. Armbruster, Nucl. Instr. and Meth. 137(1976)103.

[3] I. Bacho, D. D. Bogdanov, Sh. Daroczy, V. A. Karnaukov, L. A. Petrov and G. M. Ter-Akop'yan, JINR p13-4453(1969).

[4] A. Ghiorso, M. Leino, S. Yashita, L. Frank, P. Armbruster, J. -P. Dufour and P. K. Lemmertz, Ann. Rept. of LBL, LBL-15955(1984).

[5] N. Bohr and J. Lindhard, Mat. Fys. Medd. Dan. Vid. Selsk. 28, no. 7(1954).

[6] P. Armbruster, J. Eidens, J. W. Gruter, H. Lawin, E. Rockl and K. Sistemich, Nucl. Instr. and Meth. 91(1971)499.

[7] P. Sigmund and K. B. Winterbon, Nucl. Instr. and Meth. 119(1974)541., A. D. Marwick and P. Sigmund, Nucl. instr. and Meth. 126(1975)317. and P. Sigmund, J. Heinemeier, F. Besenbacher, P. Hvelplund and H. Knudsen, Nucl. Instr. and Meth. 150(1978)221.

[8] H. Knudsen, H. K. Haugen and P. Hvelplund, Phys. Rev. A23(1981)597.

[9] L. A. Petrov, V. A. Karnaukov and D. D. Bogdanov, JETP 32(1971)1042.

Table 1

Characteristics of dipole and quadrupole magnets of the present GARIS. See fig. 1 for D, Q1, Q2, Q3 and Q4.

	Dipole magnet	Quadrupole magnet		
	D	Q1	Q2	Q3 and Q4
Deflection angle (degrees)	20	-	-	-
Maximum field (Ts)	1.2	-	-	-
Maximum field gradient (Ts/m)	-	30	10	8
Pole length (mm)	698.1	200	200	200
Pole gap or bore radius (mm)	70.	30.5	55	55
Radius of curvature (mm)	2000	-	-	-
Maximum ampere-turn/pole (AT)	36000	13780	16000	10680
Number of turn/pole (turns)	72	53	64	534
Maximum current (A)	500	260	250	20
Total resistance of coil at 20°C (Ω)	0.07	0.07	0.09	5.7
Maximum power dissipation (KW)	17.5	4.7	5.6	2.3
Flowing rate of cooling water (l/min)	14.5	4.4	4.3	3.0
Weight (kg)	2100	200	250	650

Table 2

Experimental parameters and results. $\bar{E}$ and Δp are the mean energy and the momentum spread, respectively, after passing through the Ni-foil. The $\bar{v}/v_0$ is the average ionic velocity in unit of v_0 at the midpoint of the dipole magnet after correction of the energy loss by helium gas. The given average charge is the one at the He pressure (p_{He}) which corresponds to the minimum $B\rho$-resolution.

Ion (Beam Energy)	Ni-foil thickness (mg/cm^2)	$\bar{E}$ (MeV)	$\bar{v}/v_0$	$\Delta p/\bar{p}$ (%)	p_{He} (torr)	$\bar{q}$ (e)
^{16}O (33MeV)	2.21	22.89	6.81	3.87	13.0	6.61±0.52
^{16}O (26MeV)	2.21	15.06	5.53	6.50	6.0	5.67±0.41
^{40}Ar (38MeV)	1.77	17.90	3.85	18.3	3.0	6.11±0.34
^{68}As	1.77	3.60	1.35	111.0	0.75	2.72±0.31

Figure Captions

Fig. 1 A plan view of the present GARIS. Q1, Q2, Q3, and Q4 are quadrupole magnets and D is a dipole magnet.

Fig. 2 The charge-distribution spectra of ^{16}O (E=33 MeV) after passing the nickel window measured without gas (a), at helium pressure of 0.53 torr (b) and at 12.75 torr (c). The intensity of each spectrum is given in arbitrary unit.

Fig. 3 The measured dependence of $B\rho$-resolution on helium pressure for ^{16}O ions at 22.95 MeV (a) and at 15.1 MeV (b). The other experimental parameters are given in table 2. The experimental errors are about 10 % for all points. A solid curve shows the calculated values explained in the text.

Fig. 4 The measured dependence of $B\rho$-resolution on helium pressure for ^{40}Ar ions at 17.9 MeV. The other experimental parameters are given in table 2. The experimental errors are about 10 % for all points. A solid curve shows the calculated values explained in the text.

Fig. 5 The measured dependence of $B\rho$-resolution on helium pressure for ^{68}As ions at 3.6 MeV. The other experimental parameters are given in table 2. The

experimental errors are about 10 % for all points. A solid curve shows the calculated values explained in the text.

Fig. 6 The measured average charges obtained in helium gas of low pressure as a function of atomic numbers. Experimental values of ^{16}O, ^{40}Ar, ^{68}As, ^{84}Kr, ^{90}Mo, ^{103}Ag, ^{110}Sn, ^{132}Xe, ^{125}Cs and ^{149}Tb are plotted. The values from ^{84}Kr to ^{149}Tb are taken from ref. [9]. All the experimental points are normalized on those of the ionic velocity of $v=4v_0$ ($v_0=c/137$). A solid line shows $\bar{q} \propto z^{0.57}$ dependence.

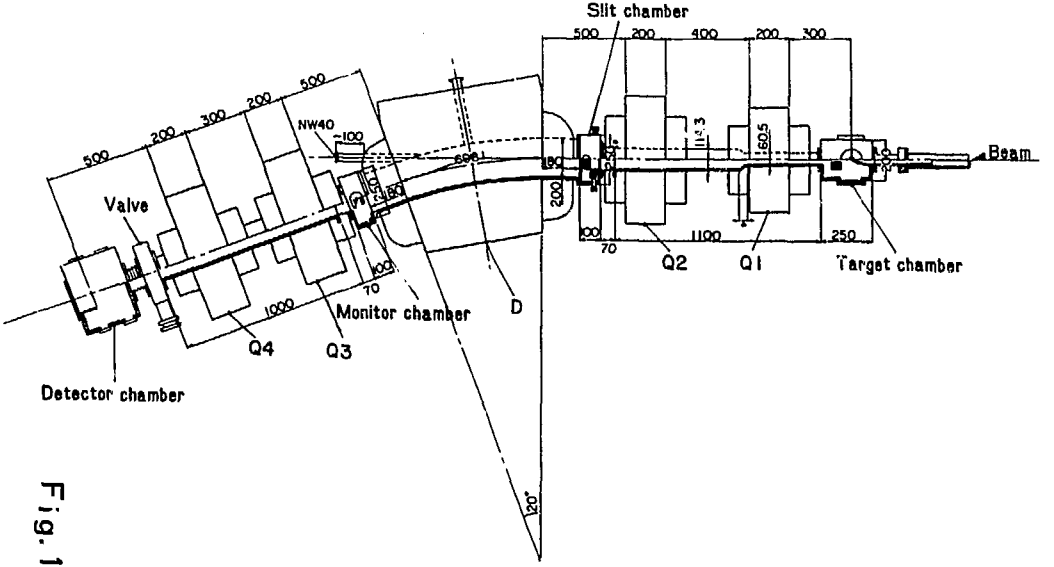
Slit chamber
500
200
400
200
300
NW40
~100
500
200
300
200
500
Valve
Beam
160.5
113
190
200
200
70
1100
250
Q2
Q1
Target chamber
Monitor chamber
D
Q4
Q3
1000
70
Detector chamber
120°

Fig. 1

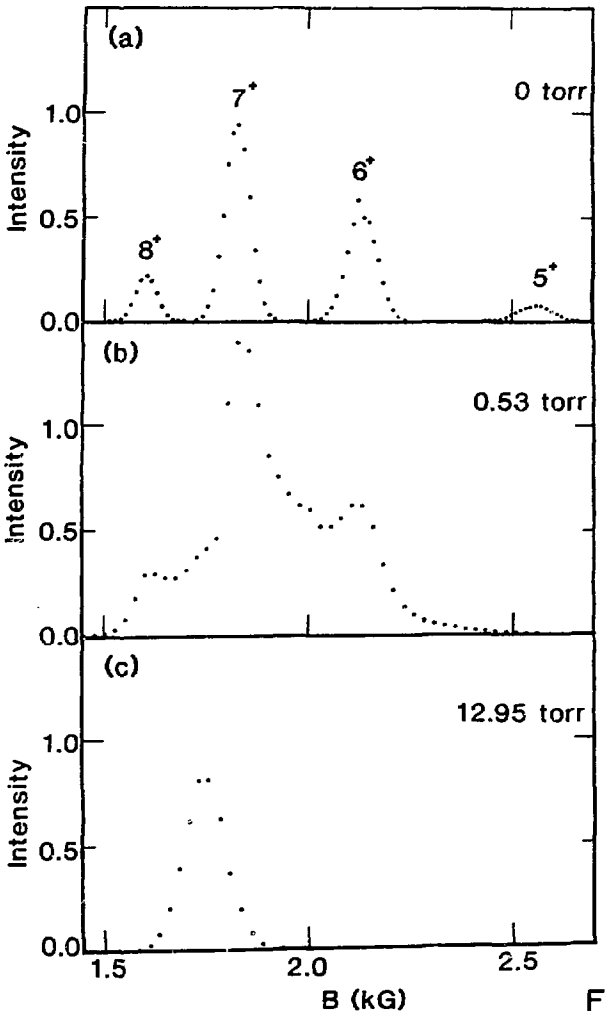
(a)
0 torr
7+
6+
8+
5+
Intensity
1.0
0.5
0.0
(b)
0.53 torr
Intensity
1.0
0.5
0.0
(c)
12.95 torr
Intensity
1.0
0.5
0.0
1.5
2.0
2.5
B (kG)

Fig. 2

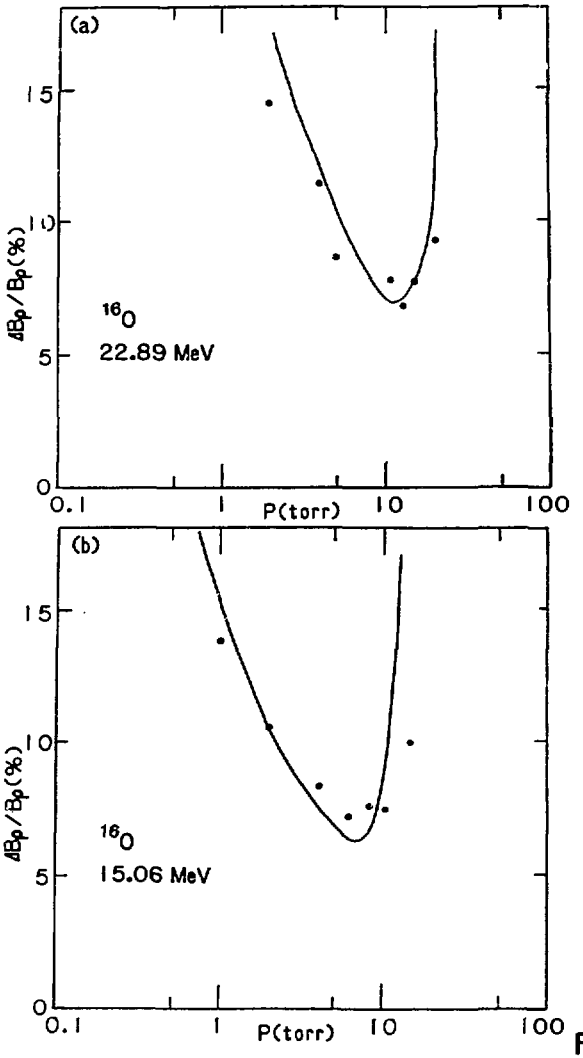
(a)
15
10
5
0
ΔBρ/Bρ(%)
16O
22.89 MeV
0.1
1
P(torr)
10
100
(b)
15
10
5
0
ΔBρ/Bρ(%)
16O
15.06 MeV
0.1
1
P(torr)
10
100

Fig. 3

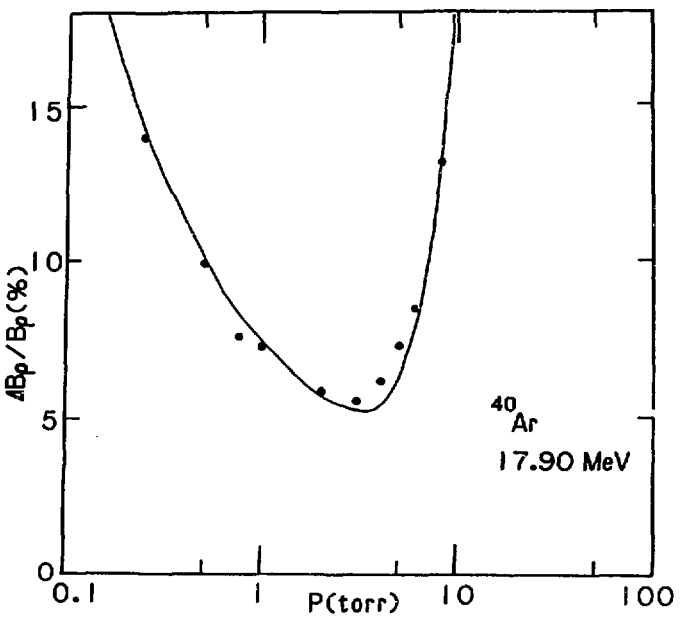

Fig. 4

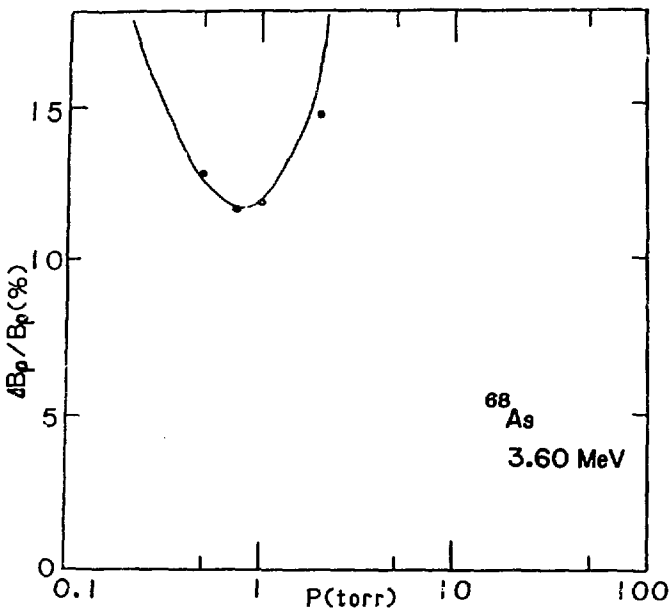

Fig. 5

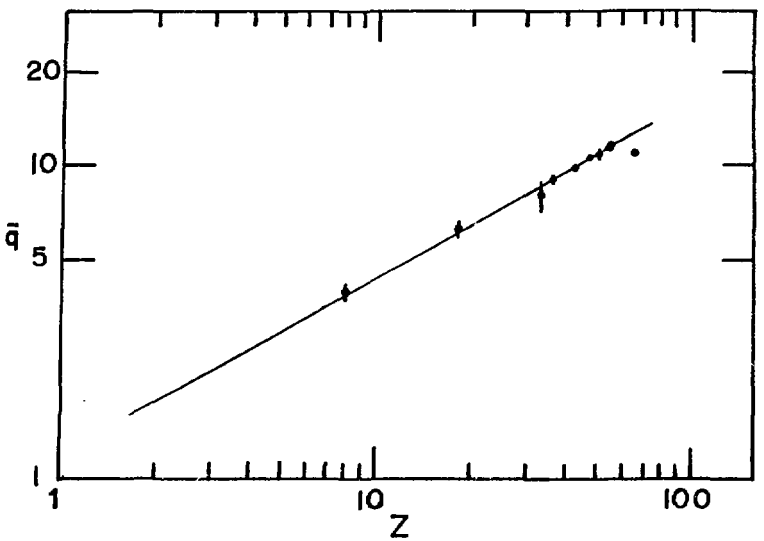

Fig. 6